On the collision rate of small particles in isotropic turbulence. II. Finite inertia case

Yong Zhou, Anthony S. Wexler, and Lian-Ping Wang[a)]
Department of Mechanical Engineering, 126 Spencer Laboratory, University of Delaware, Newark, Delaware 19716-3140

(Received 25 March 1997; accepted 21 January 1998)

Numerical experiments have been performed to study the geometric collision rate of heavy particles with finite inertia. The turbulent flow was generated by direct numerical integration of the full Navier-Stokes equations. The collision kernel peaked at a particle response time between the Kolmogorov and the large-eddy turnover times, implying that both the large-scale and small-scale fluid motions contribute, although in very different manners, to the collision rate. Both numerical results for frozen turbulent fields and a stochastic theory show that the collision kernel approaches the kinetic theory of Abrahamson [Chem. Eng. Sci. **30**, 1371 (1975)] only at very large τ_p/T_e, where τ_p is the particle response time and T_e is the flow integral time scale. Our results agree with those of Sundaram and Collins [J. Fluid Mech. **335**, 75 (1997)] for an evolving flow. A rapid increase of the collision kernel with the particle response time was observed for small τ_p/τ_k, where τ_k is the flow Kolmogorov time scale. A small inertia of $\tau_p/\tau_k=0.5$ can lead to an order of magnitude increase in the collision kernel relative to the zero-inertia particles. A scaling law for the collision kernel at small τ_p/τ_k was proposed and confirmed numerically by varying the particle size, inertial response time, and flow Reynolds number. A leading-order theory for small τ_p/τ_k was developed, showing that the enhanced collision is mainly a result of the nonuniform particle concentration that results from the interaction of heavy particles with local flow microstructures. © *1998 American Institute of Physics.* [S1070-6631(98)01305-1]

I. INTRODUCTION

Small solid particles and droplets are often dispersed, transported, and mixed by turbulent flow in many natural and industrial processes. Turbulence can enhance the coagulation rate among particles in a concentrated suspension in at least three ways. If the particles are sufficiently small in size and their inertia relative to the fluid motion negligible, the local shear in turbulence determines completely the collision process (the shear mechanism).[1] For heavy particles in vigorous turbulence, particle inertia becomes significant and collisions then arise from the differing inertial response of polydisperse particles to local fluid motion (the accelerative mechanism).[2] The turbulent shear may also increase the collision efficiencies of small particles by an order of magnitude through alteration of local relative motion between particles.[3]

In this paper, we consider only the geometric collisions of small, monodisperse particles in turbulence. We shall assume that the particles are small, with diameter d_p typically on the order of or less than the Kolmogorov length scale $\eta \equiv (\nu^3/\bar{\epsilon})^{1/4}$, where ν and $\bar{\epsilon}$ are fluid kinematic viscosity and the average rate of energy dissipation per unit mass respectively. In such cases, the local shear rate around a particle is assumed to be uniform and equal to the local velocity gradient, any deviation from this assumption (namely, the size effect) is negligible as long as only the geometric collision rate is of concern.[4] The particle density ρ_p is much larger than the fluid density ρ so that the particle inertial response time

$$\tau_p = \frac{\rho_p}{\rho}\frac{d_p^2}{18\nu}, \tag{1}$$

may be comparable to the flow Kolmogorov time scale $\tau_k = (\nu/\bar{\epsilon})^{1/2}$. For example, in cumulus clouds[5] the average dissipation rate can be on the order of 200 cm^2/s^3, 40 μm droplets would have a time scale ratio $\tau_p/\tau_k \approx 0.2$ and a size $d_p/\eta \approx 0.06$. In many engineering applications, the dissipation rate is usually much larger than in clouds, so that τ_p may even be comparable to the large-eddy time scale and the particle inertia becomes a key factor in the collision process. The term *inertia effect* shall be used to represent all aspects of the particle motion in response to the changes of the local fluid motion in a finite time τ_p due to particle inertia.

There is another reason to believe that the inertial effect, even for small τ_p, can enhance the collision rate to a level much larger than that described previously. It has been shown recently that the intense vortex tube structures, which characterize the dissipation-range dynamics in fully developed turbulence, lead to a nonuniform particle concentration field. This so-called inertial bias or preferential concentration in turbulence was first illustrated by Maxey[6] and then demonstrated by Squires and Eaton,[7] Wang and Maxey[8] through direct numerical simulations. The inertial bias was found to

[a)]Corresponding author: Department of Mechanical Engineering, 126 Spencer Laboratory, University of Delaware, Newark, Delaware 19716-3140. Phone: (302) 831-8160; Fax: (302) 831-3619; Electronic mail: LWANG@ME.UDEL.EDU

follow a Kolmogorov scaling, namely, being most effective in producing a nonuniform concentration when $\tau_p/\tau_k \sim 1$. Unlike the case of negligible particle inertia where the local strain rate plays the dominant role, the inertial bias is caused by both the local vorticity and strain rate variations.

Consider a monodisperse system consisting of N_p particles in a volume Ω, the collision rate per unit volume, $\mathcal{N}_c$, is given by

$$\mathcal{N}_c = \Gamma \frac{n_0^2}{2}, \tag{2}$$

provided that $N_p \gg 1$, where $n_0 \equiv N_p/\Omega$ is the average particle number concentration in the volume and Γ is the collision kernel. Saffman and Turner[9] first considered simultaneously the effects of the shear mechanism, the accelerative mechanism, and the gravitational mechanism on the collision kernel Γ under the assumptions that $d_p \ll \eta$, $\tau_p \ll \tau_k$, and the particle concentration field was uniform. Their results show that the accelerative mechanism gives a nonzero contribution to the collision kernel only if two colliding particles have different inertias. This work was followed by a number of studies, all done in the context of stochastical theory of turbulence, where the effect of local flow structures on the particle concentration was not explicitly considered. These include Panchev[10] for the case of τ_p spanning over τ_k, Williams and Crane[11] for intermediate-inertia particles with $\tau_k < \tau_p < T_e$, and Abrahamson[12] for very large particles with $\tau_p > T_e$, where T_e is the time scale of energy-containing eddies. Yuu,[13] Kruis and Kusters[14] considered the combined effect of local shear and unequal inertial response times on the collision rate for arbitrary τ_p. The key in the stochastical theory is to identify the proper range of scales of motion in the fluid turbulence which contribute most actively to the relative velocity between two colliding particles. In these efforts, closure assumption of one type or another was usually assumed in order to derive an expression for the average particle relative velocity. Also the particle concentration field was assumed to be uniform.

Our main objective here is to study the effect of the inertial bias on the collision rate, using numerical simulations and asymptotic analysis. In part 1 of this work,[4] we have clarified the formulation of Saffman and Turner[9] for the zero-inertia case. We intend to extend this formulation to finite-inertia particles with a nonuniform concentration field. Consistent with recent studies,[15,16] we find that the collision kernel increases rapidly with τ_p for $\tau_p/\tau_k < 1$. This will be shown to result mainly from the nonuniform particle concentration field due to the inertial bias. A scaling law for the collision kernel will be proposed and examined numerically by varying particle size, inertial response time, and flow Reynolds number. Of significance is the observation that a small particle inertia of $\tau_p/\tau_k \sim 0.5$ can lead to an order of magnitude increase in the collision kernel. Most of the numerical experiments in this work were performed for frozen flow fields. We note that more results for the evolving flow case were reported by Sundaram and Collins.[15] It is noted that there is no quantitative difference in *collision kernel* between frozen and evolving flows under the two limiting cases, namely, very small particle inertial response time and very large inertia response time. Both the simulation results and analyses in the present paper focused on these limiting cases, and, therefore, are expected to be representative of the evolving flow case as well.

The paper is organized as follows. The next section provides the details of the flow simulation and particle tracking. The numerical collision kernels for arbitrary τ_p are presented first in Sec. III. In Sec. IV we describe a scaling law and compare it with numerical results. A leading order analysis for small τ_p/τ_k is developed in Sec. V and compared to the simulation results. While most simulations utilized a frozen turbulence field, the results in an evolving turbulence are briefly discussed in Sec. VI. Finally main conclusions are drawn in Sec. VII.

II. NUMERICAL SIMULATION

A. Flow field

A homogeneous and isotropic turbulent flow was generated by full numerical simulations using a pseudo-spectral method. The incompressible Navier-Stokes equations

$$\frac{\partial \mathbf{u}}{\partial t} = \mathbf{u} \times \boldsymbol{\omega} - \nabla \left(\frac{P}{\rho} + \frac{1}{2}\mathbf{u}^2 \right) + \nu \nabla^2 \mathbf{u} + \mathbf{f}(\mathbf{x},t), \tag{3}$$

were solved along with the continuity equation $\nabla \cdot \mathbf{u} = 0$ in a periodic box of side 2π. Here $\boldsymbol{\omega} \equiv \nabla \times \mathbf{u}$ is the vorticity, P is the pressure. The time evolution was computed by applying a second-order Adams-Bashforth scheme to the nonlinear terms and a second-order Crank-Nicholson scheme for the viscous terms. The pressure was eliminated through the continuity equation.

The flow was generated from rest by the random forcing term $\mathbf{f}(\mathbf{x},t)$ which is nonzero only at low wave numbers, $|\mathbf{k}| < \sqrt{8}$. Nonlinear interactions propagate energy from low to high wave numbers and eventually viscous dissipation becomes active, leading to a quasi-steady balance of the forcing energy and the viscous dissipation.

For most discussions in this paper, the flow was frozen after the statistically stationary stage was reached, and particles were then introduced into the flow. The start of particle release will be denoted as $t = 0$. This provides us an identical flow microstructure for different runs with various particle parameters. The case of evolving flow will be considered in Sec. VI.

Since all the important flow scales are resolved in a full numerical simulation, the grid resolution determines the scale separation, and thus the Reynolds number of the resulting flow. Various grid resolutions from 32^3 to 128^3 were used to provide a range of Taylor microscale Reynolds number (Table I).

Table I lists the flow parameters (from top to bottom): the component rms fluctuating velocity u', average dissipation rate $\overline{\epsilon}$, viscosity ν, Taylor microscale Reynolds number $R_\lambda \equiv u'\lambda/\nu$ (where λ is the transverse Taylor microscale $\lambda \equiv u'/\sqrt{\langle (\partial u_1/\partial x_1)^2 \rangle}$), Kolmogorov length η, time scale τ_k, large-eddy turnover time $T_e \equiv u'^2/\overline{\epsilon}$, the time scale ratio T_e/τ_k, collision radius R (which is equal to the particle di-

TABLE I. Flow characteristics and parameters for the particle system.

Grid resolution	32^3	64^3	96^3	128^3
u'	17.02	18.22	18.30	18.64
$\overline{\epsilon}$	3568.8	3421.0	3554.7	3374.4
ν	0.6000	0.2381	0.1387	0.09450
R_λ	24	45	59	75
η	0.0882	0.0450	0.0294	0.0224
τ_k	0.0130	0.00830	0.00625	0.00529
T_e	0.081	0.097	0.094	0.103
T_e/τ_k	6.23	11.7	15.0	19.5
R/η	1.78	1.0/0.5	1.0/0.5	1.0/0.5
N_p	1024/2048	2048/3072	2640/4096	3072/5120
$\phi(\times 10^4)$	84/168	4.00/0.74	1.40/0.27	0.73/0.15

ameter for a monodisperse system), total number of particles N_p, and particle volume fraction ϕ. Other details of the simulated flows can be found in Wang and Maxey.[8]

B. Particle motion

We consider the motion of heavy spherical particles in a nonuniform turbulent flow. The particle is assumed to be small in comparison with the Kolmogorov microscale of the turbulence and the loading dilute enough that the presence of the particles does not modify the base turbulence. Under the assumption that the density of the particle ρ_p is much larger than the density of the fluid ρ, and that a quasi-steady Stokes drag can be used, the equation of motion for a heavy particle becomes

$$\frac{d\mathbf{V}(t)}{dt}=\frac{\mathbf{u}(\mathbf{Y}(t),t)-\mathbf{V}(t)}{\tau_p}, \tag{4}$$

where $\mathbf{V}(t)$ and $\mathbf{Y}(t)$ are the velocity and the center position of a heavy particle, respectively. The body force is neglected since we focus solely on inertia-induced collisions. The combined effects of inertia and gravitational settling will be considered separately.

The location and velocity of each particle were advanced while the flow field was either frozen or continued to evolve in time. A fourth-order Adams-Bashforth method was used to integrate the particle equation of motion. The fluid velocity at the location of a particle was interpolated from the values at neighboring grids using a 6-point Lagrange interpolation. Typically $10^3 \sim 10^4$ particles were introduced at $t=0$ into the computational domain at random initial positions with an initial velocity equal to the local fluid velocity. After about $3\tau_p$, any effects of the initial conditions on the particle motion became lost. The simulation was continued for at least $13\tau_p$ or 4 to 5 large-eddy turnover times during which collision counts and other statistical averages were taken. It should be noted that the particle concentration field and the local-in-time collision kernels (defined in Sec. II C below) may not reach their asymptotic, statistically stationary stage at $t=3\tau_p$ since the local accumulation process is affected by large-scale fluid motion.[8] On the other hand, in practical applications one may be more interested in the particle collision statistics shortly after the particle release rather than the asymptotic value. With this in mind and for the purpose of obtaining a small numerical uncertainty, we take $t=3\tau_p$ as the starting time for all statistical averages. A change of the starting time to $t=2T_e$ showed that the results change less than 20% and are unchanged qualitatively.

C. Collision detection

The collision detection algorithm was described in Part 1 of this work[4] and will not be repeated here. It was shown that three different collision counting schemes could be applied and each gave slightly different numerical collision kernels for zero-inertia particles. These schemes differ in the choice of particle system used for collision counting. They are summarized here:

Scheme 1. Particles were allowed to overlap in the system at the beginning of a time step and were not removed from the system after collision. This scheme was shown in Part 1 to be the only scheme that is consistent with the Saffman and Turner[9] formulation.

Scheme 2. At the beginning of each time step, the overlapping particles were marked and excluded from collision detection. Therefore, the actual number of particles used for collision detection was less than the total number of particles used and varied in time.

Scheme 3. Particles were removed immediately from the system when they collide. As a result, the total number of particles decreased with time and particles remaining in the system were nonoverlapping at the beginning of each time step. This scheme closely represents reality if both the collision efficiency and coagulation efficiency are close to one, since two particles upon collision will form a particle of larger size and as such will disappear from the current size group.

For each of the three schemes, one can define a local-in-time collision kernel for any time step dt as

$$\Gamma_i(t^{(n)})=\frac{2\Omega N_c(t^{(n)}\rightarrow t^{(n+1)})}{dt[N_{pi}(t^{(n)})]^2}, \tag{5}$$

where $i=1$, 2, and 3 denotes the individual schemes, $N_c(t^{(n)}\rightarrow t^{(n+1)})\approx \mathcal{N}_c\Omega\ dt$ is the total collision count in the time step $t^{(n)}<t\leqslant t^{(n+1)}$, $N_{pi}(t^{(n)})$ is the total number of particles participating in collision detection and is given for each scheme as

$$N_{pi}(t^{(n)})=\begin{cases} N_p=\text{const}, & \text{for } i=1; \\ N_p-2N_0(t^{(n)}), & \text{for } i=2; \\ N_p(t^{(n)}), & \text{for } i=3; \end{cases} \tag{6}$$

where $N_0(t^{(n)})$ is the number of overlapping pairs at $t^{(n)}$ in scheme 2, $N_p(t^{(n)})$ is the number of particles left in the system in scheme 3. It is assumed that particle volume fraction is very small so that binary collisions dominate. These local-in-time collision kernels were quite *noisy* if N_p is not very large. They can be improved by averaging over different realizations of turbulence field and initial particle locations. A further average over time gives the final collision kernel $\langle\Gamma_i\rangle$.

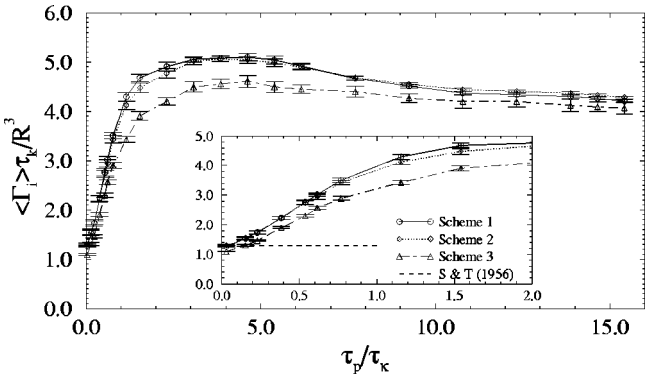

FIG. 1. Numerical collision kernels, normalized by R^3/τ_k, as a function of the particle response time over the Kolmogorov time scale. For this set of simulations, parameters were set to: $dt=0.001$, $R=0.8\Delta x$, grid resolution is 32^3. $N_p=1024$ for schemes 1 and 2, while N_p was increased to 2048 for scheme 3 to achieve comparable uncertainty intervals. The error bars indicate the 95% confidence intervals. The horizontal line in the insert denotes the Saffman and Turner result $\Gamma\tau_k/R^3=1.294$.

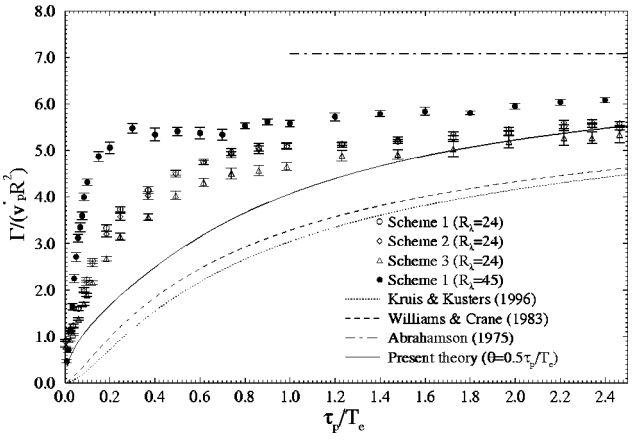

FIG. 2. Numerical collision kernels over the particle fluctuation velocity v_p', as a function of the particle response time over the large-eddy turnover time T_e. The error bars indicate the 95% confidence intervals. The Abrahamson[12] prediction is $\Gamma/(v_p'R^2)=4\sqrt{\pi}=7.09$.

III. NUMERICAL RESULTS FOR ARBITRARY INERTIA

Figure 1 shows the numerical collision kernels, normalized by R^3/τ_k, as a function of τ_p/τ_k in a frozen turbulence at $R_\lambda=24$. The error bars denote the 95% numerical confidence intervals, which were estimated based on 21 runs with independent realizations of particle initial locations. We observe that qualitatively the three collision counting schemes yield similar results. The collision kernels increase very rapidly for small τ_p/τ_k, reach a peak at $\tau_p/\tau_k\approx 4$ or $\tau_p/T_e\approx 0.6$, and then drop slowly with increasing τ_p/τ_k. The same qualitative behavior was found by Sundaram and Collins,[15] although they assumed a perfectly elastic collision of nonoverlapping particles (their post-collision treatment is close to, but not exactly the same as, our scheme 2). The peak reflects both the effects of small and large scales of fluid motion. The inertial bias produces a nonuniform particle concentration. This small-scale effect[8] can enhance the collision kernel significantly (see Sec. V) and is scaled on the Kolmogorov time scale. On the other hand, as τ_p increases, particle velocities fail to correlate at collision and the larger scale fluid motion becomes more relevant in determining the relative velocity between two particles. This causes an increase in the relative velocity between two particles and a concomitant increase in the collision kernel. This latter effect is likely to scale with the integral time scale of the flow. The question of how the location of this peak changes with the flow Reynolds number remains to be examined with simulations at higher flow Reynolds numbers.

Schemes 1 and 2 result in almost the same collision kernel values, as expected for this low volume fraction system.[4] For zero-inertia particles ($\tau_p=0$), scheme 1 gives the same value as the Saffman and Turner[9] result. A close examination seems to suggest that scheme 1 gives a slightly larger kernel for $\tau_p/\tau_k<7$ while scheme 2 gives a larger kernel for $\tau_p/\tau_k>7$, but the difference is not significant statistically. Scheme 3, on the other hand, yields a collision kernel 10% to 15% less than the other two schemes, due to a preferential removal as discussed in Part 1.[4]

Figure 2 replots the results in a manner that can be easily compared with the theory of Abrahamson[12] for large τ_p/T_e. Also included in this figure are results at higher flow Reynolds number (64^3 grid simulations). Here $v_p'\equiv\sqrt{\langle V_iV_i/3\rangle}$ is the rms particle fluctuating velocity. We note that $\langle\Gamma\rangle/(v_p'R^2)$ increases monotonically with τ_p/T_e. This can be explained as follows. Let $v_r^{(1)}$ and $v_r^{(2)}$ be the longitudinal velocities of the two particles at collision. Assuming the relative velocity $w_r\equiv v_r^{(2)}-v_r^{(1)}$ between two colliding particles follows a Gaussian distribution with a standard deviation σ_w and the particle concentration is uniform, then $\langle|w_r|\rangle=\sqrt{2/\pi}\sigma_w$. The collision kernel for scheme 1 is

$$\langle\Gamma_1\rangle=2\pi R^2\langle|w_r|\rangle=2\sqrt{2\pi}R^2\sigma_w. \tag{7}$$

Defining the correlation coefficient of the particle velocities as $\rho_{12}\equiv\langle v_r^{(1)}v_r^{(2)}\rangle/(v_p')^2$, we can express σ_w as

$$\sigma_w=\sqrt{\langle w_r^2\rangle}=\sqrt{2}v_p'\sqrt{1-\rho_{12}}. \tag{8}$$

It follows that

$$\frac{\langle\Gamma_1\rangle}{v_p'R^2}=4\sqrt{\pi}\sqrt{1-\rho_{12}}. \tag{9}$$

This reduces precisely to the Abrahamson[12] result if $\rho_{12}=0$. In general, we can argue that the correlation coefficient ρ_{12} decreases monotonically with τ_p, since particle velocities depend more and more on their history of travel and thus nonlocal fluid motion as τ_p increases. Consequently, $\langle\Gamma_1\rangle/(v_p'R^2)$ increases monotonically. Of significance is that the numerical collision kernels at $\tau_p/T_e=2.5$ are about 22% and 14% less than Abrahamson's prediction for $R_\lambda=24$ and $R_\lambda=45$, respectively, implying that there is still a significant velocity correlation.

An estimate of ρ_{12} as a function of τ_p/T_e can be made by treating the fluid velocity around a particle as a simple Monte-Carlo process (see the Appendix). Substituting Eqn. (A8) into (9), we have

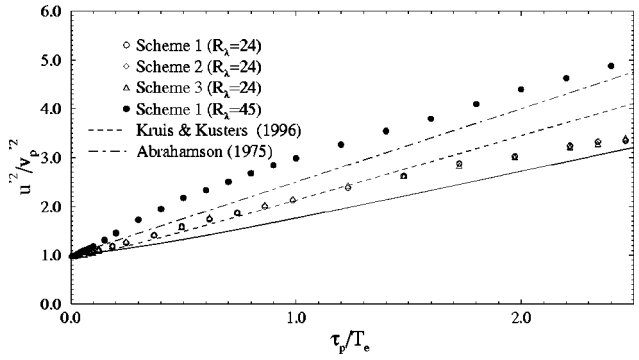

FIG. 3. The ratio of fluid to particle kinetic energy as a function of τ_p/T_e.

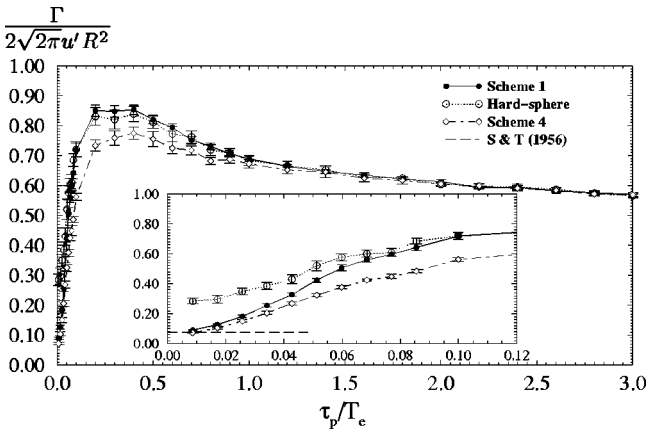

FIG. 4. Numerical collision kernels, normalized by $2\sqrt{2\pi}u'R^2$, as a function of the particle response time over the integral time scale. For this set of simulations, parameters were set to: $dt=0.001$, $R=0.458\Delta x$, grid resolution is 64^3. $N_p=2048$. The error bars indicate the 95% confidence intervals. The horizontal line in the insert denotes the Saffman and Turner result $\Gamma/(2\sqrt{2\pi}u'R^2)=0.0767$.

$$\frac{\langle\Gamma_1\rangle}{v_p'R^2}=2\sqrt{2\pi}\left[1-\exp\left(-\frac{1}{\theta}\right)\right]\times\sqrt{\frac{\theta}{1-\theta[1-\exp(-1/\theta)]}},\tag{10}$$

where $\theta=0.5\tau_p/T_e$. This result may be viewed as an improvement over that of Abrahamson,[12] and is plotted in Fig. 2. Interestingly, Eqn. (10) shows a reasonable comparison with the numerical results for $\tau_p/T_e>1.5$. Furthermore Eqn. (10) indicates that ρ_{12} diminishes slowly (in an algebraic manner, see (A9)) for large τ_p/T_e. For example, $\sqrt{1-\rho_{12}}=0.937$ at $\tau_p/T_e=10$, thus the difference between Eqn. (10) and Abrahamson's result is still noticeable at $\tau_p/T_e=10$. For $\tau_p/T_e<1.5$, Eqn. (10) predicts a smaller value than the numerical results, particularly for the $R_\lambda=45$ case. The difference can be viewed as the effect of the nonuniform particle concentration (see Sec. V). Also shown are the predictions of Kruis and Kusters,[14] Williams and Crane[11] (see the Appendix). Interestingly, all the theoretical results are similar in shape. The present theory seems to be slightly better than other theories. However, one should keep in mind that in the development of the other theories, the flow Reynolds number was assumed to be large. Furthermore, empirical constants such as the one used to relate the Lagrangian time scale T_L to T_e may be adjusted in the works of Kruis and Kusters,[14] Williams and Crane[11] to better match the numerical results.

The ratio of fluid to particle kinetic energy is shown in Fig. 3 as a function of τ_p/T_e. A simple stochastic analysis would predict a linear curve (for example, Abrahamson,[12] Williams and Crane[11]). Figure 3 shows that the curves are not exactly linear, but rather the slope drops slowly as τ_p/T_e increases. The average slope is very close to one at large τ_p/T_e, in agreement with the previous theories.[11,12] Also shown in the figure are our result, Eqn. (A4), using a simple stochastic analysis, and the results of Abrahamson,[12] Kruis and Kusters.[14] They all give a reasonable although not very accurate prediction.

To further examine the effect of collision detection schemes on the numerical collision kernel, we compare in Fig. 4 results based on scheme 1 and two other schemes. Scheme 4[4] is a more realistic scheme in which particles are relocated after collisions to represent generation of particles in the current size group due to the coagulation of smaller particles in a stationary system. In our simulations using scheme 4, we introduced more particles at the beginning of the simulations and only used a portion of the particles for the collision calculation. Particles involved in a collision were replaced by those particles not previously used in the collision calculation, so as to keep the system stationary and to maintain the preferential concentration at the same time. Scheme 4 gives almost the same results at very small and large τ_p/T_e, but can possibly result in collision kernels 5% to 10% smaller than those of scheme 1 for intermediate particle inertia. Also shown are results based on the hard-sphere model used previously by Sundaram and Collins[15] in which a perfectly elastic collision model without friction is used to calculate the particle velocities after a collision. We note that while there is essentially no difference between the hard-sphere model results and those of scheme 1 for $\tau_p/T_e>0.1$, the hard-sphere model can lead to a collision kernel much larger than the Saffman and Turner[9] prediction in the limit of $\tau_p/T_e\to 0$. This latter difference is due to artificial repeated collisions in the hard-sphere model as noted by Sundaram and Collins.[15]

IV. THE SCALING LAW FOR Γ AT SMALL τ_p

In the following, we shall focus on particles with small inertia, $\tau_p/\tau_k<1$. In this case, particles will respond to the change of local large-scale fluid motion rather quickly. As a consequence, we expect that the dissipation-range fluid dynamics dominates the collision process. If, in addition, particle size or the collision radius R is much smaller than the integral length scale of the turbulence and the flow Reynolds number is sufficiently large, we can argue that the collision kernel Γ depends only on the collision radius R, the average dissipation rate $\overline{\epsilon}$, the kinematic viscosity ν, and the particle response time τ_p. Then we can write

$$\Gamma=f(R,\overline{\epsilon},\nu,\tau_p).\tag{11}$$

A dimensional analysis would lead to

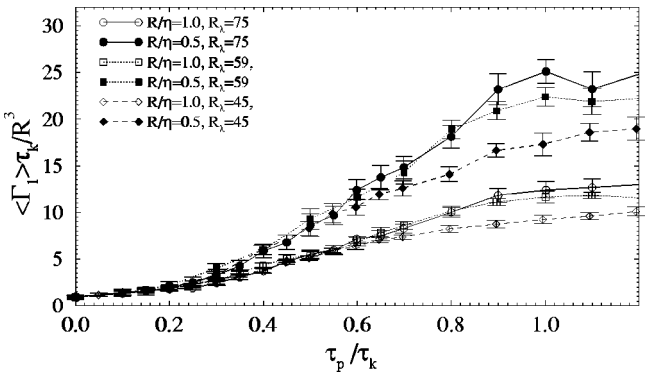

FIG. 5. Numerical collision kernels, normalized by R^3/τ_k, as a function of τ_p/τ_k. The error bars indicate ± standard deviation. The important parameters for these runs are shown in Table I.

$$\frac{\Gamma}{R^3/\tau_k} = f\left(\frac{\tau_p}{\tau_k}, \frac{R}{\eta}\right), \tag{12}$$

where $\tau_k = (\nu/\bar{\epsilon})^{1/2}$ is the Kolmogorov time scale, $\eta = (\nu^3/\bar{\epsilon})^{1/4}$ is the Kolmogorov length scale.

Therefore, when we consider small inertia and small size effects, the dimensionless collision kernel is a function of the dimensionless particle response time (or Stokes number) and the dimensionless collision radius. In the limit of $\tau_p/\tau_k \to 0$ and $R/\eta \to 0$, Eqn. (12) is consistent with the Saffman and Turner[9] result for zero-inertia particles, with $f(0,0) = 1.294$. Eqn. (12) is essentially a Kolmogorov scaling in high-Reynolds number turbulence.

To confirm the above scaling law, we performed a series of numerical simulations by varying the following three parameters one at a time: the Stokes number τ_p/τ_k, the dimensionless collision radius R/η, and the flow Reynolds number. The results are summarized in Fig. 5. Since in the last section we showed that the results were similar for different collision counting schemes, we shall use scheme 1 only for the rest of discussions in this paper. Several interesting observations can be made for Fig. 5.

First, the nondimensional collision kernels do not show a dependence on the flow Reynolds number R_λ for $\tau_p/\tau_k < 0.6$, even though the Reynolds numbers are not high in our simulations. For the two higher Reynolds number cases, the range of validity of the scaling law extends to $\tau_p/\tau_k < 0.8$. For larger τ_p/τ_k, particles start to interact with a range of flow time scales, including the large-scale motions which depend on the flow Reynolds number. Since the fluid motion at larger scales is more fully represented in higher Reynolds number flow, the contribution of larger scale fluid motion to the collision kernel is increased. As a result, the collision kernel increases with R_λ (or equivalently τ_p/T_e) for larger τ_p/τ_k. We speculate that the range of validity of the scaling law would be extended further, should these simulations be done at even higher Reynolds numbers. These observations support the proposed scaling law.

Second, as $\tau_p/\tau_k \to 0$, the numerically-derived collision kernels all approach the Saffman and Turner[9] prediction, $\Gamma = 1.294 R^3/\tau_k$, independent of the flow Reynolds number. Note that the Gaussian probability distribution for the velocity gradient is a reasonable approximation for low Reynolds number flows and the finite size effect for $R/\eta \leqslant 1$ is negligible.[4]

Third, for non-zero τ_p/τ_k, the nondimensional collision kernel decreases as R/η increases. This is expected since the history effect, namely the relative particle motion before the two particles are brought to a distance R apart, increasingly influences the relative velocity at collision. Particles respond to scales of motion larger than R. For small R in the far dissipation range, the relative fluid velocity scales as R, while in the inertial subrange it is scaled as $R^{1/3}$ (see Kolmogorov[17]). The mean shear rate between two particles then decreases with R for a given τ_p. Therefore, the normalized collision kernel drops as the collision radius increases.

The most significant observation is that the numerically-derived collision kernels increase very rapidly with the particle response time. Even for a small $\tau_p/\tau_k = 0.5$ for which the scaling law is applicable, the collision kernel is about 1 order of magnitude larger than the value for zero-inertia particles when $R/\eta = 0.5$. This rapid increase cannot be explained by any of the previous theories. We shall study this rapid increase analytically in the next section.

V. A LEADING-ORDER ANALYSIS FOR SMALL τ_p

Our objective here is to shed some light on the observed rapid increase of Γ with τ_p for small τ_p. We will apply the results of an asymptotic analysis developed by Maxey[6] for small τ_p, that accounts for the nonuniform concentration effect due to the inertial bias.

If we assume that $\tau_p/\tau_k < 1$, τ_k represents the smallest time scale in the flow and the particles must respond very quickly to any local change of fluid motion. Consequently, the particle velocity is completely specified by its instantaneous position, to leading order in τ_p/τ_k. This allows us to define a particle velocity field $\mathbf{v}(\mathbf{x},t)$ which is given by[6]

$$\mathbf{v}(\mathbf{x},t) = \mathbf{u}(\mathbf{x},t) - \tau_p\left(\frac{\partial \mathbf{u}}{\partial t} + \mathbf{u}\cdot\nabla\mathbf{u}\right), \tag{13}$$

in the absence of body forces.

Maxey[6] pointed out that this particle velocity field, unlike the fluid velocity field, is not incompressible. The divergence field of the particle velocity is

$$\nabla\cdot\mathbf{v} = -\tau_p \frac{\partial u_j}{\partial x_i}\frac{\partial u_i}{\partial x_j} = -\tau_p\left(s_{ij}s_{ij} - \frac{\omega^2}{2}\right), \tag{14}$$

where $\boldsymbol{\omega} = \nabla\times\mathbf{u}$ and $s_{ij} = (\partial u_i/\partial x_j + \partial u_j/\partial x_i)/2$ are the local fluid vorticity and rate of strain field, respectively. It follows that particles will accumulate in regions of low vorticity and high strain rate. Maxey[6] showed that the local particle number concentration, $n(\mathbf{x},t)$, after a uniform release at $t=0$, would evolve as

$$n(\mathbf{x},t) = n_0 \exp\left\{\tau_p \int_0^t \left[s_{ij}s_{ij} - \frac{\omega^2}{2}\right](\mathbf{Y}(t';\mathbf{x},t),t')\,dt'\right\}, \tag{15}$$

where the integrand $[s_{ij}s_{ij} - (\omega^2/2)]$ in the above expression should be evaluated following the trajectory of a particle whose position would be at $\mathbf{x}$ at time t. We note that the

integrand can take both positive and negative values and as such may cancel in the integration over the history of the particle trajectory. Therefore, we argue that the main contribution to the integral comes from the part of trajectory with $t' \approx t$, or local in space relative to $\mathbf{x}$. We thus propose the following approximation to (15):

$$n(\mathbf{x},t) \approx n_0 \exp\left\{ \tau_p \tau_f \left(s_{ij} s_{ij} - \frac{\omega^2}{2} \right) \right\}, \tag{16}$$

where τ_f is a history time scale to be determined, and to leading order is only a property of the flow. Since τ_p is very small, the leading order expansion for $n(\mathbf{x},t)$ is

$$n(\mathbf{x},t) \approx n_0 \left\{ 1 + \tau_p \tau_f \left(s_{ij} s_{ij} - \frac{\omega^2}{2} \right) \right\}. \tag{17}$$

In the context of the scaling law discussed in the last section, we expect that τ_f be directly related to τ_k. We will use Eqn. (17) as it is more consistent with the leading order approximation, however, Eqn. (17) cannot be applied to very high vorticity regions as it may lead to negative local concentration for a given τ_f. To circumvent this, we simply set the local concentration to zero if Eqn. (17) becomes negative. Equations (16) and (17) do reflect correctly the qualitative connection between the local particle concentration and the local vorticity or strain rate.

We shall now combine the above results to derive a leading order approximation for the average collision kernel. We start by introducing a local-in-space collision kernel $\Gamma(\mathbf{x},t)$ as

$$\Gamma(\mathbf{x},t) = \frac{\dot{\mathcal{N}}(\mathbf{x},t)}{n^2(\mathbf{x},t)/2} = \int_{\Omega_R} (-w_r^-) \mathrm{d}\Omega. \tag{18}$$

The relative velocity w_r has been partitioned into two parts, a positive part and a negative part, according to

$$w_r^- = \begin{cases} 0, & \text{if } w_r \geqslant 0, \\ w_r, & \text{if } w_r < 0; \end{cases} \quad w_r^+ = \begin{cases} w_r, & \text{if } w_r \geqslant 0, \\ 0, & \text{if } w_r < 0. \end{cases} \tag{19}$$

Since

$$\int_{\Omega_R} |w_r| \mathrm{d}\Omega = \int_{\Omega_R} w_r^+ \mathrm{d}\Omega - \int_{\Omega_R} w_r^- \mathrm{d}\Omega, \tag{20}$$

$$\int_{V_R} \nabla \cdot \mathbf{w} \mathrm{d}V = \int_{\Omega_R} \mathbf{w} \cdot \mathrm{d}\vec{\Omega} = \int_{\Omega_R} w_r^+ \mathrm{d}\Omega + \int_{\Omega_R} w_r^- \mathrm{d}\Omega, \tag{21}$$

it follows that

$$\Gamma(\mathbf{x},t) = \int_{\Omega_R} (-w_r^-) \mathrm{d}\Omega = \frac{1}{2} \int_{\Omega_R} |w_r| \mathrm{d}\Omega - \frac{1}{2} \int_{V_R} \nabla \cdot \mathbf{w} \mathrm{d}V, \tag{22}$$

where V_R is the volume of the sphere with radius R centered on $\mathbf{x}$.

If the collision radius R is small compared to η and the flow is locally isotropic, the first integral in (22) can be written as

$$\frac{1}{2} \int_{\Omega_R} |w_r| \mathrm{d}\Omega \approx 2\pi R^3 \left| \frac{\partial v_1}{\partial x_1} \right| = 2\pi R^3 \left| \frac{\partial u_1}{\partial x_1} - \tau_p \frac{\partial}{\partial x_1} \left(\frac{\partial u_1}{\partial t} + \mathbf{u} \cdot \nabla u_1 \right) \right|, \tag{23}$$

using Eqn. (13). The second term may be rewritten as

$$\frac{1}{2} \int_{V_R} \nabla \cdot \mathbf{w} \mathrm{d}V = \frac{1}{2} V_R \overline{\nabla \cdot \mathbf{w}} = -\frac{1}{2} V_R \tau_p R \frac{\partial}{\partial x_1} \overline{\left[s_{ij} s_{ij} - \frac{\omega^2}{2} \right]}, \tag{24}$$

where the overbar denotes a local average over the spherical volume V_R. Therefore the local collision kernel can be expressed as

$$\Gamma(\mathbf{x},t) = 2\pi R^3 \left| \frac{\partial u_1}{\partial x_1} - \tau_p \frac{\partial}{\partial x_1} \left(\frac{\partial u_1}{\partial t} + \mathbf{u} \cdot \nabla u_1 \right) \right| + \frac{1}{2} V_R \tau_p R \frac{\partial}{\partial x_1} \overline{\left[s_{ij} s_{ij} - \frac{\omega^2}{2} \right]}. \tag{25}$$

The average collision kernel is related to both the local collision kernel and the local particle number concentration as

$$\langle \Gamma \rangle = \frac{\langle \dot{\mathcal{N}}(\mathbf{x},t) \rangle}{n_0^2/2} = \frac{\langle \Gamma(\mathbf{x},t) n^2(\mathbf{x},t) \rangle}{n_0^2}, \tag{26}$$

where the angle brackets denote a spatial average over the entire computational domain, and $n_0 = \langle n(\mathbf{x},t) \rangle$ is the average concentration. Substituting (17) and (25) into (26) and dropping the local averaging as a first approximation for small R, we obtain

$$\langle \Gamma \rangle = 2\pi R^3 \left\langle \left| \frac{\partial u_1}{\partial x_1} - \tau_p \frac{\partial}{\partial x_1} \left(\frac{\partial u_1}{\partial t} + \mathbf{u} \cdot \nabla u_1 \right) \right| \times \left[1 + \tau_p \tau_f \left(s_{ij} s_{ij} - \frac{\omega^2}{2} \right) \right]^2 \right\rangle + \frac{2\pi R^3}{3} \tau_p \left\langle R \frac{\partial}{\partial x_1} \times \left(s_{ij} s_{ij} - \frac{\omega^2}{2} \right) \left[1 + \tau_p \tau_f \left(s_{ij} s_{ij} - \frac{\omega^2}{2} \right) \right]^2 \right\rangle. \tag{27}$$

Several remarks regarding Eqn. (27) can be made here. In a direct numerical simulation, the full nonuniform flow field is simulated, so all the terms in Eqn. (27) can be computed directly. The first part inside the absolute signs of the first term includes the leading order correction to the relative velocity gradient. The second part enclosed by the square brackets represents the effect of nonuniform particle concentration due to the inertial bias. If we neglect the effect of nonuniform particle concentration or equivalently set the second part to one, the collision kernel will increase but very slowly with τ_p due to the first part or the effect of particle inertia on the particle relative velocity. The important point to note is that the two parts in the first term of (27) are *positively* correlated, namely, both high local concentration and high local relative velocity are found in regions of high strain rate. The combined effect is then a much higher average collision kernel than what one would have if the particle concentration were uniform. Similar observations can be

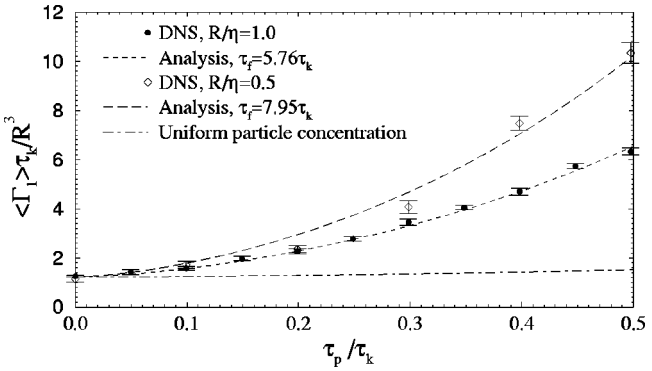

FIG. 6. Comparison of the asymptotic analysis, Eqn. (27), with numerical results for small particle response time $\tau_p/\tau_k<0.5$. The error bars indicate $\pm$ standard deviation. Grid resolution is 64^3, $R_\lambda=45$.

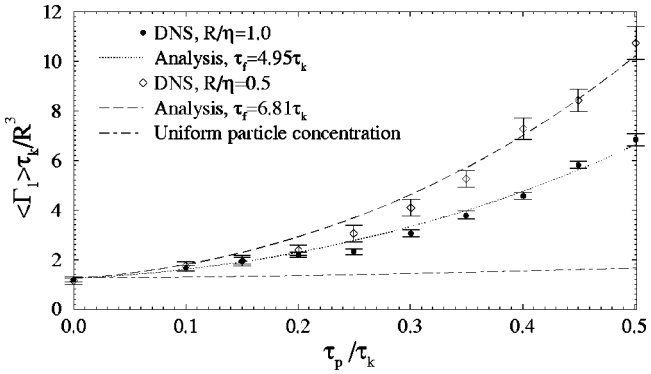

FIG. 8. Comparison of the asymptotic analysis, Eqn. (27), with numerical results for small particle response time $\tau_p/\tau_k<0.5$. The error bars indicate $\pm$ standard deviation. Grid resolution is 128^3, $R_\lambda=75$.

made for the second term in (27). We note, however, that the second term would not make any net contribution to $\langle\Gamma\rangle$ under the uniform concentration approximation since the volume average of $(s_{ij}s_{ij}-(\omega^2/2))$ is zero, but it does make a positive contribution when the nonuniform concentration effect is considered. Finally, Eqn. (27) is essentially consistent with the scaling law (12) if the history characteristic time τ_f scales with τ_k. If the particle concentration were uniform, Eqn. (27) would become

$$\langle\Gamma_u\rangle=2\pi R^3\left\langle\left|\frac{\partial u_1}{\partial x_1}-\tau_p\frac{\partial}{\partial x_1}\left(\frac{\partial u_1}{\partial t}+\mathbf{u}\cdot\nabla u_1\right)\right|\right\rangle. \qquad (28)$$

We can now fit the approximation (27) to the numerical results in Fig. 5 for the region $\tau_k/\tau_p<0.5$ for which the scaling law is justified. A least square procedure (minimizing the square error between the analysis and the simulation results in the region $\tau_p/\tau_k<0.5$) was used to deduce the best value of τ_f. The comparisons of the numerical results and the approximation (27) are shown in Figs. 6, 7 and 8 for the three flow Reynolds numbers. We conclude that Eqn. (27) predicts the shape of $\langle\Gamma_1\rangle$ versus τ_p observed in the numerical simulations despite all the approximations involved in deriving (27). Also shown in these figures are the predictions under the uniform concentration approximation, Eqn. (28), which yield a much smaller $\langle\Gamma_1\rangle$ value than the numerical results. Therefore, the nonuniform concentration resulting from finite particle inertia is the dominant factor rapidly increasing the collision kernel at small τ_p/τ_k.

Figure 9 shows the value of τ_f, normalized by τ_k, as a function of the flow Reynolds number R_λ and R/η. For a given R/η, τ_f/τ_k is only weakly dependent of R_λ. For the range of R_λ covered in the simulations, τ_f/τ_k is changed by about 16%, which is much less than the T_e/τ_k variation (see Table I). Therefore, we may conclude that τ_f scales with τ_k. The difference in τ_f/τ_k between the two R/η values is somewhat larger, but part of this difference is due to the finite size effect which is not included in Eqn. (27).

VI. RESULTS IN EVOLVING FLOW

The numerical results considered so far were obtained using turbulent fields that did not evolve in time. Here we present some preliminary results for an evolving turbulence field at $R_\lambda\approx45$ for small τ_k. Figure 10 compares the results with those obtained in a frozen turbulence at the same flow Reynolds number. Note that for the evolving flow the Kolmogorov time scale τ_k varies in time so an average value over time was used in Fig. 10. For $\tau_p\to0$, the frozen and evolving flow fields yield the same collision kernel, implying that the formulation of Saffman and Turner[9] is valid for the collision of fluid elements in an evolving flow.[4] However, as τ_p/τ_k increases, the collision kernel in the evolving flow

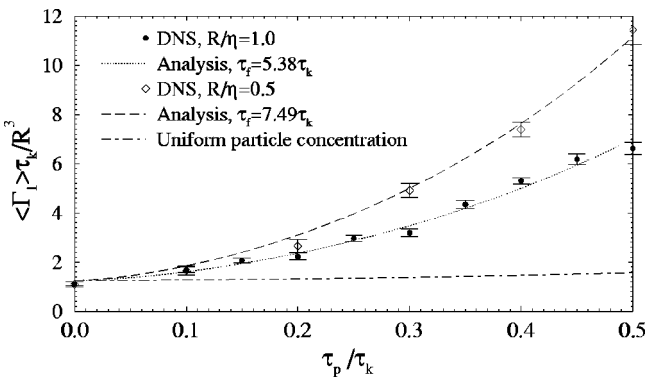

FIG. 7. Comparison of the asymptotic analysis, Eqn. (27), with numerical results for small particle response time $\tau_p/\tau_k<0.5$. The error bars indicate $\pm$ standard deviation. Grid resolution is 96^3, $R_\lambda=59$.

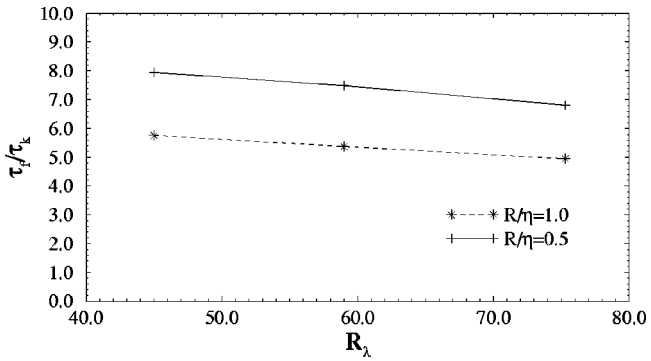

FIG. 9. The history time scale τ_f, normalized by the Kolmogorov time scale τ_k, as a function of the Taylor microscale Reynolds number R_λ.

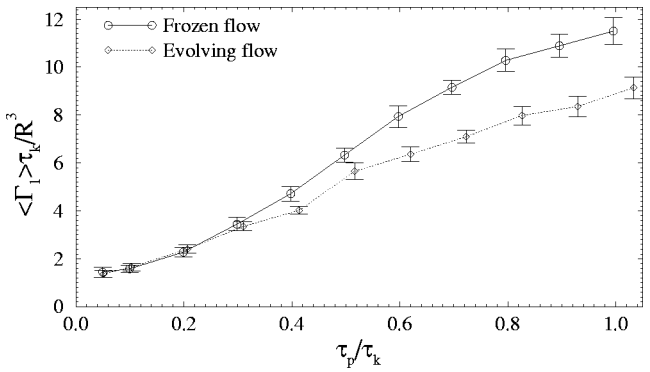

FIG. 10. The numerical collision kernels in an evolving flow and a frozen turbulence as a function of τ_p/τ_k. Grid resolution is 64^3, $R_\lambda = 45$. The error bars denote the 95% numerical confidence intervals.

deviates from that in the frozen flow, and is always less than the latter. At $\tau_p/\tau_k = 1$, the reduction is about 20%. The physical explanation is that heavy particles respond to a range of eddies that evolve both in time and space, the temporal evolution of the flow tends to reduce the fluid velocity correlation or persistence of a given local flow structure around a particle. For small τ_p/τ_k, this effect can lower the level of local particle accumulation and thus the average collision kernel. The observed reduction, however, does not alter the qualitative behavior of the collision kernel at small τ_p/τ_k.

We are in the process of collecting more data for the evolving flow, covering a wider range of τ_p and the flow Reynolds number. It should be noted that more results for the evolving flow case are reported recently by Sundaram and Collins.[15] Our preliminary results agree with those of Sundaram and Collins[15] qualitatively in general. It is noted that there is no quantitative difference in *collision kernel* between frozen and evolving flows under the two limiting cases, namely, very small particle inertial response time and very large inertia response time. Both the simulation results and analyses in the present paper focused on these limiting cases, and, therefore, are expected to be representative of the evolving flow case as well. There are significant quantitative differences for the intermediate inertia case, which will be a topic of future study. It may be useful to note that a passive scalar field advected by Gaussian, frozen, and evolving velocity fields shows different spectra and dynamics.[18,19]

Therefore, the dynamical features of the fluid velocity field should be considered carefully for the collision process.

VII. SUMMARY

Numerical experiments were conducted to study the geometric collision rate of heavy particles with finite inertia. It was found that the collision kernel reached a peak at a particle response time larger than the Kolmogorov time but less than the large-eddy turnover time. This indicates that both the large-scale and small-scale fluid motion can contribute, although in very different manners, to the collision rate. This is consistent with the observation of Sundaram and Collins[15] on particle collision in an evolving flow. The ratio of the collision kernel to particle fluctuating velocity, $\langle\Gamma\rangle/v_p'$, on the other hand, increases monotonically with τ_p, implying that the large scale effect dominates the change of the collision kernel for most τ_p. Simulations at higher flow Reynolds numbers are necessary to further clarify the proper scaling of the maximum collision rate.

In the limit of zero inertia ($\tau_p/\tau_k \to 0$), the analytical result of Saffman and Turner[9] provides a useful estimate for the collision kernel but a finite correction to their result must be made if a realistic collision counting scheme is employed.[4] On the other hand, for very large particles ($\tau_p/T_e \gg 1$), the kinetic theory of Abrahamson[12] is expected to apply. Our simulations show that the numerically-derived collision kernel is still significantly less than Abrahamson's prediction at $\tau_p/T_e = 2.5$, and that his prediction is only approached at extremely large τ_p/T_e. This was also shown by a simple stochastic theory in which the fluid velocity on a particle was treated as a Monte-Carlo process.

For small τ_p/τ_k, which is most relevant to atmospheric contexts, the collision kernel increases very quickly with τ_p/τ_k. A scaling law for the collision kernel for this limit was proposed and confirmed by numerical simulations. The rapid increase of the collision kernel was shown, by an asymptotic analysis, to result mainly from the nonuniform particle concentration field due to the inertial bias. Of significance is the observation that a small inertia with $\tau_p/\tau_k = 0.5$ may lead to an order of magnitude increase in the collision rate.

Most of the results were obtained in a frozen turbulent flow. Preliminary results for an evolving flow indicate that the non-persistence of flow structure may reduce the collision rate. This is expected, at least for small τ_p/τ_k, since the level of local particle accumulation is somewhat reduced in an evolving turbulence. Further work is necessary to systematically study this effect.

It should be noted that most previous studies show a non-zero contribution of the particle inertia to the collision kernel only through unequal or differential inertia in a polydisperse system. Here we have demonstrated that even in a monodisperse system, the particle inertia must be considered to accurately describe the collision kernel. For equal-size particles, the inertial effect alters the collision rate in at least four ways in addition to the shear mechanism: (a) by a response to the local fluid acceleration in addition to the local fluid velocity, through which the local *spatial variation* in the fluid acceleration can modify the relative velocity (e.g., Eqn. (13)); (b) by the lack of correlation of fluid velocity and fluid acceleration on the particle trajectories which can affect the relative velocity due to the combined effect of particle inertia and both the *spatial and temporal variations* of the flow field; (c) by the local particle accumulation as a result of the inertial bias, and (d) by different initial conditions with which the particles are released into the flow. For finite particle inertia, all these are no longer a local phenomena, but rather depend on both the spatial and temporal variations of the turbulence. The present numerical and analytical results will help us to develop a better and more complete theory which can combine all the above aspects and be applied to arbitrary particle inertia.

ACKNOWLEDGMENTS

This work was supported by the University of Delaware Research Foundation, the IBM Watson Research Center, and the State of Delaware. L.P.W. is grateful to Professors Martin Maxey, Lance Collins, and Renwei Mei for several helpful discussions in the course of this work.

APPENDIX: A SIMPLE STOCHASTIC ANALYSIS OF TWO-PARTICLE VELOCITY CORRELATION

Here we present a simple stochastic analysis to gain a qualitative understanding of the two-particle velocity correlation coefficient ρ_{12} introduced in Sec. III. We shall treat the particle motion as a succession of interactions with turbulent eddies, where each eddy has constant flow properties. More specifically, we consider a one-dimensional version of the particle equation of motion

$$\frac{dv(t)}{dt}=\frac{u-v}{\tau_p}, \tag{A1}$$

where the fluid velocity u is treated as a Monte-Carlo process with a fixed eddy life time T.[20] The fluid velocity will take a Gaussian random value in each eddy with a standard deviation equal to the rms fluid fluctuation velocity u'. It can be shown that the particle velocity variance $(v_p')^2$ is related to the fluid velocity correlation $R_f(\tau)\equiv\langle u(t)u(t+\tau)\rangle$ by[21]

$$(v_p')^2\equiv\langle v^2(t)\rangle=\frac{1}{\tau_p}\int_0^\infty R_f(\tau)\exp\left(-\frac{\tau}{\tau_p}\right)d\tau. \tag{A2}$$

For a Monte-Carlo process R_f is a triangle function[20]

$$R_f(\tau)=\begin{cases} u'^2\left(1-\dfrac{\tau}{T}\right), & \text{for } |\tau|<T;\\ 0, & \text{for } |\tau|\geqslant T. \end{cases} \tag{A3}$$

Substituting (A3) into (A2), we obtain a relationship between the particle and fluid kinetic energy

$$\frac{(v_p')^2}{u'^2}=1-\theta\left[1-\exp\left(-\frac{1}{\theta}\right)\right], \tag{A4}$$

where $\theta\equiv\tau_p/T$.

Now we would like to estimate the velocity correlation between two colliding particles, $\langle v^{(1)}v^{(2)}\rangle$. If the particle size is very small, the two particles must be found in a same eddy upon collision. We further assume that the two particles enter the eddy at a same time,[22] say, $t=0$. Then by integrating Eqn. (A1) the particle velocities can be written as

$$v^{(i)}(t)=u_e\left[1-\exp\left(-\frac{t}{\tau_p}\right)\right]+v^{(i)}(0)\exp\left(-\frac{t}{\tau_p}\right),$$
$$\text{for } 0<t<T, \quad i=1,2; \tag{A5}$$

where $v^{(i)}(0)$ denotes the particle velocity at $t=0$, and u_e is the eddy velocity. Before entering the eddy $(t<0)$, the two particles interact independently with different eddies so that $\langle v^{(1)}(0)v^{(2)}(0)\rangle=\langle v^{(1)}(0)u_e\rangle=\langle v^{(2)}(0)u_e\rangle=0$. If the probability distribution for the two particles to collide in the time interval $0<t<T$ is uniform, then the velocity correlation is

$$\langle v^{(1)}v^{(2)}\rangle=\frac{1}{T}\int_0^T\langle v^{(1)}(t)v^{(2)}(t)\rangle dt. \tag{A6}$$

Substituting (A5) into (A6), we have

$$\frac{\langle v^{(1)}v^{(2)}\rangle}{u'^2}=1-2\theta\left[1-\exp\left(-\frac{1}{\theta}\right)\right]+\frac{\theta}{2}\left[1-\exp\left(-\frac{2}{\theta}\right)\right]. \tag{A7}$$

The essential physics is that the particle velocities must be partially correlated due to interactions with a same eddy right before collision, and that the level of correlation depends on how quickly the particles can respond to the new fluid velocity in the eddy. Finally, combining (A4) and (A7), we obtain

$$\rho_{12}=1-\frac{\theta}{2}\frac{\left[1-\exp\left(-\dfrac{1}{\theta}\right)\right]^2}{\left\{1-\theta\left[1-\exp\left(-\dfrac{1}{\theta}\right)\right]\right\}}. \tag{A8}$$

Equation (A8) shows that ρ_{12} decreases monotonically with θ. In particular, the following asymptotic behaviors are obtained

$$\rho_{12}=\begin{cases} 1-\dfrac{\theta}{2}, & \text{for } \theta\ll 1;\\ \dfrac{2}{3\theta}, & \text{for } \theta\gg 1. \end{cases} \tag{A9}$$

In Sec. III, the results for arbitrary inertia were presented in terms of τ_p/T_e, where T_e is the eddy turnover time. T_e may also be viewed as the integral time scale of the turbulence. The form of the velocity correlation (A3) implies that $T/2=T_e$, therefore, we set

$$\theta=0.5\frac{\tau_p}{T_e} \tag{A10}$$

when the above analysis was compared to the numerical results in Sec. III.

It should be noted that the above analysis does not include the eddy size effect, which can modify the particle-eddy interaction time as the particles may traverse the eddy in a time less than T. Also the shear mechanism is not considered.

Finally we cite here the recent results by Kruis and Kusters[14] when applied to equal size particles with $\rho_p\gg\rho$. They gave the following expression for the ratio of the particle and fluid kinetic energy

$$\frac{(v_p')^2}{u'^2}=\frac{1+(\gamma+1)\zeta}{(1+\zeta)(1+\gamma\zeta)}, \tag{A11}$$

where

$$\zeta\equiv 2.5\frac{\tau_p}{T_e}, \quad \gamma\equiv 0.183\left(\frac{u'}{v_k}\right)^2. \tag{A12}$$

Equation (A11) differs from (A4) as it is a function of two independent dimensionless parameters. Note that (A11) was first derived by Williams and Crane[11] but with a different definition for γ. Williams and Crane[11] assumed that $\gamma \gg 1$ and used a simpler form under that limit. For equal size particles, Kruis and Kusters' result for the collision kernel becomes

$$\frac{\Gamma}{v_p'} = 4\sqrt{\pi}R^2 \sqrt{\frac{\gamma\zeta^2}{(1+\zeta)(1+\gamma\zeta)}} \times \sqrt{\left(1-\frac{\sqrt{1+2\zeta}}{1+\zeta}\right)\left(\frac{2+(\gamma+1)\zeta}{1+(\gamma+1)\zeta}\right)}. \tag{A13}$$

Note that (A13) reduces to the result of Williams and Crane[11] if $\gamma \gg 1$, which is

$$\frac{\Gamma}{v_p'} = 4\sqrt{\pi}R^2 \sqrt{\frac{\zeta}{1+\zeta}} \sqrt{1-\frac{\sqrt{1+2\zeta}}{1+\zeta}}. \tag{A14}$$

If, in addition, we assume $\zeta \gg 1$, then the Abrahamson's result is recovered.

Finally, we note that for large τ_p/T_e our theory approaches Abrahamson's result Γ_A in the following manner:

$$\Gamma = \Gamma_A\left[1-\frac{2T_e}{3\tau_p}\right], \tag{A15}$$

while both (A13) and (A14) yield

$$\Gamma = \Gamma_A\left[1-\sqrt{\frac{T_e}{5\tau_p}}\right] \tag{A16}$$

for large τ_p/T_e. Therefore, all the theories predict that Abrahamson's result will be approached in an algebraic manner, although our theory seems to approach Abrahamson's result more quickly.

[1]T. R. Camp and P. C. Stein, ''Velocity gradients and internal work in fluid motion,'' J. Boston Soc. Civil Eng. **30**, 219 (1943).
[2]T. W. R. East and J. S. Marshall, ''Turbulence in clouds as a factor in precipitation,'' Q. J. R. Meteorol. Soc. **80**, 26 (1954).
[3]P. R. Jonas and P. Goldsmith, ''The collection efficiencies of small droplets falling through a sheared air flow,'' J. Fluid Mech. **52**, 593 (1972).
[4]L. P. Wang, A. S. Wexler, and Y. Zhou, ''On the collision rate of small particles in isotropic turbulence. Part 1. Zero-inertia case,'' Phys. Fluids **10**, 266 (1998).
[5]J. C. Weil and R. P. Lawson, ''Relative dispersion of ice crystal in seeded cumuli,'' J. Applied Meteorol. **32**, 1055 (1993).
[6]M. R. Maxey, ''The gravitational settling of aerosol particles in homogeneous turbulence and random flow fields,'' J. Fluid Mech. **174**, 441 (1987).
[7]K. D. Squires and J. K. Eaton, ''Preferential concentration of particles by turbulence,'' Phys. Fluids A **3**, 1169 (1991).
[8]L. P. Wang and M. R. Maxey, ''Settling velocity and concentration distribution of heavy particles in homogeneous isotropic turbulence,'' J. Fluid Mech. **256**, 27 (1993).
[9]P. G. Saffman and J. S. Turner, ''On the collision of drops in turbulent clouds,'' J. Fluid Mech. **1**, 16 (1956). Also Corrigendum, J. Fluid Mech. **196**, 599 (1988).
[10]S. Panchev, *Random Function and Turbulence* (Pergamon Press, New York, 1971), pp. 301–309.
[11]J. J. E. Williams and R. I. Crane, ''Particle collision rate in turbulent flow,'' Int. J. Multiphase Flow **9**, 421 (1983).
[12]J. Abrahamson, ''Collision rates of small particles in a vigorously turbulent fluid,'' Chem. Eng. Sci. **30**, 1371 (1975).
[13]S. Yuu, ''Collision rate of small particles in a homogeneous and isotropic turbulence,'' AIChE. J. **30**, 802 (1984).
[14]F. E. Kruis and K. A. Kusters, ''The collision rate of particles in turbulent media,'' J. Aerosol Sci. **27**, S263 (1996).
[15]S. Sundaram and L. R. Collins, ''Collision statistics in an isotropic, particle-laden turbulent suspension,'' J. Fluid Mech. **335**, 75 (1997).
[16]C. Hu and R. Mei, ''Effect of inertia on the particle collision coefficient in Gaussian turbulence,'' the *7th International Symposium on Gas-Particle Flows*, Paper FEDSM 97-3608, ASME Fluids Engineering Conference (1997).
[17]A. N. Kolmogorov, ''The local structure of turbulence in incompressible viscous fluid for very large Reynolds numbers,'' Proc. R. Soc. London, Ser. A **434**, 9 (1991) [in Russian in Dokl. Akad. Nauk. SSSR **30**, 301 (1941)].
[18]J. R. Chasnov, V. M. Canuto, and R. S. Rogallo, ''Turbulence spectrum of a passive temperature field: results of a numerical simulation,'' Phys. Fluids **31**, 2065 (1988).
[19]M. Holzer and E. D. Siggia, ''Turbulent mixing of a passive scalar,'' Phys. Fluids **6**, 1820 (1994).
[20]L.-P. Wang and D. E. Stock, ''Stochastic trajectory models for turbulent diffusion: Monte-Carlo process versus Markov chains,'' Atmos. Environ. **26A**(9), 1599 (1992).
[21]L.-P. Wang and D. E. Stock, ''Dispersion of heavy particles by turbulent motion,'' J. Atmos. Sci. **50**(13), 1897 (1993).
[22]One can remove this assumption and allow the second particle enters the eddy at a different time, say, at t_1, where $0<t_1<T$. In that case, a double integration over both t and t_1 will have to be carried out to obtain the average velocity correlation, which may not yield an algebraic, analytical expression. One may also assume more realistic probability distributions for the interaction time $(t-t_1)$ and the time lag t_1. We had performed numerical integrations to test various possibilities, with the conclusion that the final result was not so sensitive to the assumptions we made here.